Evolution of superconductivity and antiferromagnetic order in Ba(Fe$_{0.92-x}$Co$_{0.08}$V$_x$)$_2$As$_2$

Jieming Sheng,[1,2,3,4] Xingguang Li,[1] Congkuan Tian ●,[1] Jianming Song ●,[5] Xin Li,[5] Guangai Sun,[5] Tianlong Xia,[1]
Jinchen Wang,[1] Juanjuan Liu,[1] Daye Xu,[1] Hongxia Zhang,[1] Xin Tong,[2,3] Wei Luo,[2,3]
Liusuo Wu,[4] Wei Bao,[1,6] and Peng Cheng[1,*]

[1]*Department of Physics and Beijing Key Laboratory of Opto-electronic Functional Materials & Micro-nano Devices,*
Renmin University of China, Beijing 100872, People's Republic of China
[2]*Institute of High Energy Physics, Chinese Academy of Sciences (CAS), Beijing 100049, People's Republic of China*
[3]*Spallation Neutron Source Science Center, Dongguan 523803, People's Republic of China*
[4]*Department of Physics, Southern University of Science and Technology, Shenzhen 518055, People's Republic of China*
[5]*Key Laboratory of Neutron Physics and Institute of Nuclear Physics and Chemistry, China Academy of Engineering Physics,*
Mianyang 621999, People's Republic of China
[6]*Department of Physics, City University of Hong Kong, Kowloon, Hong Kong SAR, People's Republic of China*

The vanadium doping effects on the superconductivity and magnetism of iron pnictides are investigated in Ba(Fe$_{0.92-x}$Co$_{0.08}$V$_x$)$_2$As$_2$ by transport, susceptibility, and neutron scattering measurements. The doping of magnetic impurity V causes a fast suppression of superconductivity with T_C reduced at a rate of approximately 7.4 K/1% V. On the other hand, for $x \geqslant 0.02$, long-range C-type antiferromagnetic order is recovered upon V doping, in contrast to the $x = 0$ sample with no detectable magnetic order. The value of ordered magnetic moments of Ba(Fe$_{0.92-x}$Co$_{0.08}$V$_x$)$_2$As$_2$ follows a domelike evolution versus doping concentration x. A possible Griffiths-type antiferromagnetic region of multiple coexisting phases in the phase diagram of Ba(Fe$_{0.92-x}$Co$_{0.08}$V$_x$)$_2$As$_2$ is identified, in accordance with previous theoretical predictions based on the cooperative behavior of magnetic impurities and conduction electrons mediating the Ruderman-Kittel-Kasuya-Yosida interactions between them.

I. INTRODUCTION

Antiferromagnetic (AFM) correlations are closely related to the unconventional superconductivity (SC) in Fe-based superconductors [1,2]. The typical parent compound BaFe$_2$As$_2$ (122) exhibits a collinear C-type AFM order and orthorhombic lattice distortion below $T_N \sim 138$ K, and superconductivity gradually emerges with suppressing both the AFM and structural transitions with charge doping [3,4]. At the same time, the evolutions of AFM order with chemical doping present rich features. For example, the AFM order changes from long-range commensurate to short-range transversely incommensurate with Co/Ni electron doping and finally disappears with the avoidance of the magnetic quantum critical point (QCP) [5,6]. On the other hand, hole doping on the Ba site with alkali metals could induce a tetragonal magnetic phase with spin reorientation and a new double-Q AFM order [7,8]. Moreover, hole doping on the Fe site with magnetic impurities Cr/Mn could generate a competing G-type AFM order and spin fluctuations [9,10]. A more recent study on BaFe$_{1.9-x}$Ni$_{0.1}$Cr$_x$As$_2$ suggests that the ordered moment and the ordered temperature of static magnetism in iron pnictides can be decoupled and tuned separately by chemical doping [11]. The above observations show the diverse responses of

Fe-based magnetism to different impurities and have been considered as valuable clues to the puzzle of a Fe-based superconducting mechanism, which has not yet been solved. Exploring different impurity effects therefore is called for.

The vanadium impurity doping effect on iron pnictides has been rarely studied until recently. In a previous work, we found that vanadium serves as a magnetic impurity and a very effective hole donor for the 122 system [12]. The avoided QCP and spin-glass state which were previously reported in the superconducting phase of Co/Ni-doped BaFe$_2$As$_2$ can also be realized in nonsuperconducting Ba(Fe$_{1-x}$V$_x$)$_2$As$_2$ [12]. A very recent transport and spectroscopy investigation on V-doped BaFe$_2$As$_2$ found evidence for the coexistence of AFM and local superconducting regions [13]. These experimental findings make vanadium an interesting impurity probe for further investigations. So far the studies of vanadium impurities only focused on the parent compound BaFe$_2$As$_2$. The influences on the superconductivity in FeAs-122 systems is still unknown.

In this paper, we report the physical properties of Ba(Fe$_{0.92-x}$Co$_{0.08}$V$_x$)$_2$As$_2$, which explore the effect of magnetic impurity V on the Ba(Fe$_{0.92}$Co$_{0.08}$)$_2$As$_2$ superconductor with a near optimal $T_C \approx 22$ K. Besides a fast suppression of superconductivity, V doping could induce a long-range C-type AFM order with a domelike evolution of the ordered moment. The onset AFM ordering temperature identified from neutron scattering measurements can be greatly enhanced (>70 K)

*pcheng@ruc.edu.cn
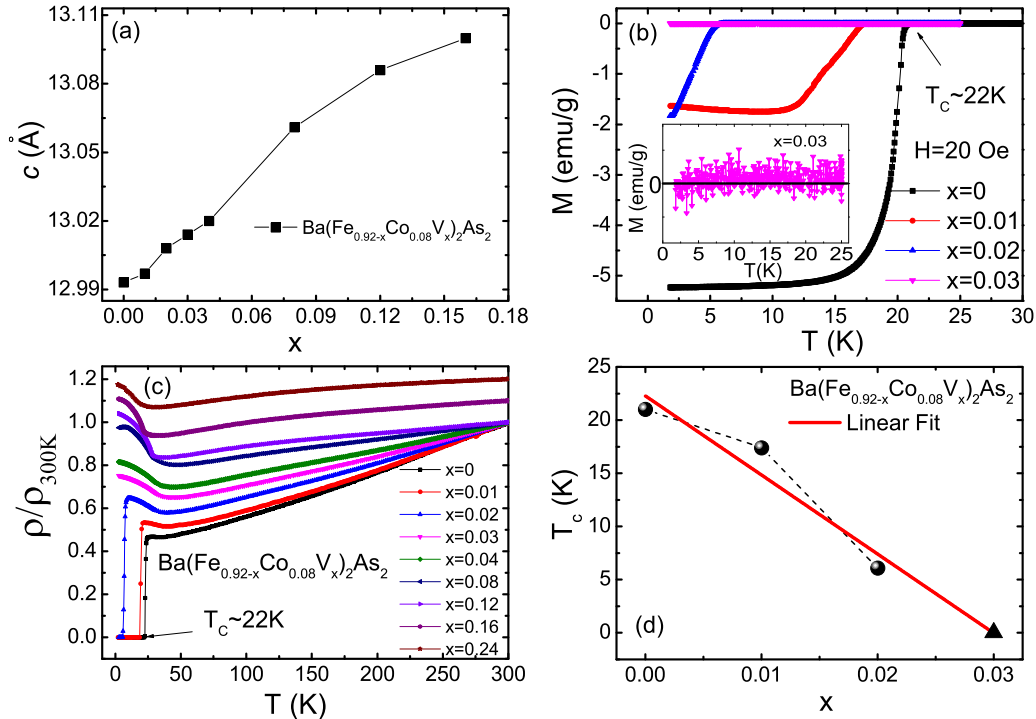
FIG. 1. (a) Room-temperature c-axis lattice parameters of the $Ba(Fe_{0.92-x}Co_{0.08}V_x)_2As_2$ series as a function of nominal V concentration x. (b) Temperature dependence of zero-field-cooling magnetic susceptibilities for $x = 0$–0.03 samples under a field of 20 Oe. (c) Temperature dependence of electrical resistivity for $Ba(Fe_{0.92-x}Co_{0.08}V_x)_2As_2$; the data are normalized to the room-temperature value. For $x = 0.16$ and $x = 0.24$, the data are shifted by a constant value of 0.1 and 0.2, respectively, for clarity. (d) The superconducting transition temperature T_C is plotted as a function of V doping concentration. The red solid line is the linear fitting result of the data.

at some certain doping concentrations, indicating possible different magnetic phases. Finally, the phase diagram of $Ba(Fe_{0.92-x}Co_{0.08}V_x)_2As_2$ is given and the underlying physics is discussed.

II. EXPERIMENTAL DETAILS

Single crystals of $Ba(Fe_{0.92-x}Co_{0.08}V_x)_2As_2$ were grown by the self-flux method similar to our previous report [12]. Crystals with nominal doping between $x = 0$ and $x = 0.36$ are obtained for x-ray, magnetization, electrical transport, and neutron scattering measurements. The x-ray diffraction patterns were collected from a Bruker D8 Advance x-ray diffractometer using Cu $K\alpha$ radiation. The magnetization measurements of our samples were performed using a Quantum Design magnetic property measurement system (MPMS3). Resistivity measurements were performed on a Quantum Design physical property measurement system (QD PPMS-14T).

Neutron scattering experiments were carried out on the Xingzhi cold neutron triple-axis spectrometer at the China Advanced Research Reactor (CARR) [14] and the Kunpeng cold neutron triple-axis spectrometer at the China Academy of Engineering Physics (CAEP). The results below are all reported using an orthorhombic structural unit cell. For each doping, a single crystal with a typical mass of 0.1–0.2 g was aligned to the $(H0L)$ scattering plane. For $x = 0.12$, the crystal was also aligned in the $(0KL)$ scattering plane, allowing for a search for a possible incommensurate AFM

phase along the b axis [$(0K0)$, transverse direction] similar to that in a previous report [5].

III. RESULTS

Figure 1(a) presents the doping-dependent c-axis lattice parameters of $Ba(Fe_{0.92-x}Co_{0.08}V_x)_2As_2$ derived from the single-crystal x-ray data. Vanadium substitution effectively expands the c axis similar to the effect that was observed in $Ba(Fe_{1-x}V_x)_2As_2$ [12].

Figure 1(b) shows the temperature dependence of DC magnetic susceptibilities for $x = 0$–0.03 samples under a field of 20 Oe. For $x = 0$, namely, $Ba(Fe_{0.92}Co_{0.08})_2As_2$, the onset transition of the Meissner effect appears at 22 K. With slight V doping, both the superconducting transition temperature T_c and the superconducting shielding volume fraction quickly decrease. The fast suppression of SC also manifests in the temperature-dependent resistivity data [Fig. 1(c)]. T_c is defined as the onset point of the Meissner effect which corresponds well to the zero-resistivity temperature determined from the R-T curve. From $x = 0$ to $x = 0.02$, the suppression of T_c possibly follows a nonlinear behavior as shown in Fig. 1(d). For $x = 0.03$, no diamagnetic signal is detected down to 1.8 K. If we assume $T_c = 0$ K for $x = 0.03$ and fit all the data linearly, the T_c suppression rate can be roughly calculated to be 7.4 K/1% V [Fig. 1(d)]. The value is similar to that in previous reports about magnetic-impurity-doped Fe-based superconductors such as V-doped LiFeAs [15], Cr-doped $Ba(Fe, Ni)_2As_2$ [16], or Mn-doped $Ba_{0.5}K_{0.5}Fe_2As_2$ [17].
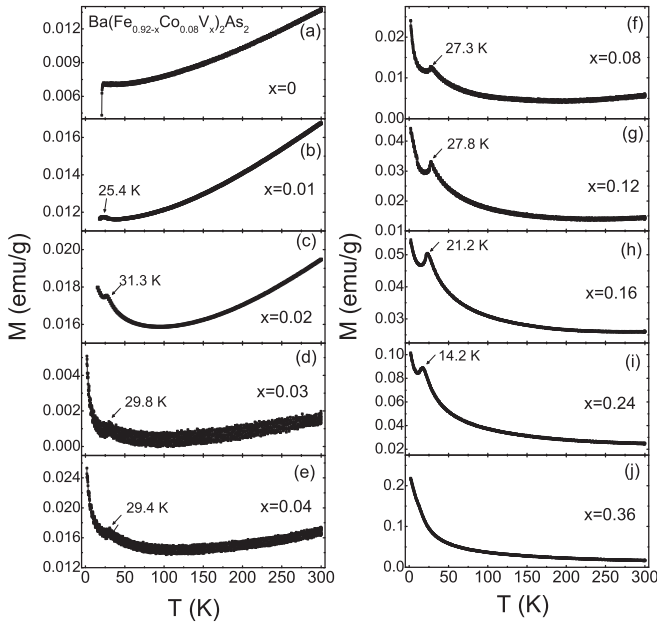
FIG. 2. (a)–(j) The temperature dependence of normal-state DC susceptibilities for the $Ba(Fe_{0.92-x}Co_{0.08}V_x)_2As_2$ series under a magnetic field of 1 T applied in the $H \parallel ab$ direction. T_N is determined by the local maxima of $M(T)$ curves (dM/dT not shown here).

FIG. 3. (a) Longitudinal ($H03$) scans at $Q_{AFM} = (103)$ and $T = 5$ K. (b) Transverse ($1K3$) scans at $Q_{AFM} = (103)$ at different temperatures for $x = 0.12$. (c) The doping-dependent ordered magnetic moments at $T = 5$ K for $Ba(Fe_{0.92-x}Co_{0.08}V_x)_2As_2$.

The temperature-dependent resistivities of all samples are shown in Fig. 1(c); an anomaly feature at around 30 K gradually emerges with increasing x. This anomaly quite resembles the resistivity anomaly caused by the AFM/structural transition in Fe-based 122 materials, which indicates a possible recovery of a stronger magnetic order in the samples. Therefore, as shown in Fig. 2, we measured the DC magnetic susceptibilities of the normal state for all samples with $H = 1$ T applied parallel to the ab plane. For $x = 0$, no sign of a magnetic transition could be detected in the susceptibility data. But for $x \geqslant 0.01$, the AFM transition features in the $M(T)$ curves emerge and get clearer and sharper with increasing x. The AFM transition temperature T_N shown in Fig. 2 is defined by the local extremum of the dM/dT curves; the resistivity anomaly temperatures could also be determined using the same method and have roughly the same values as T_N (see the final phase diagram in Fig. 5). It first increases slightly, then decreases monotonously with doping until it could not to be identified at $x = 0.36$. Another feature of $M(T)$ curves comes from the high-temperature region. It gradually evolves from a typical T-linear behavior for samples with small x to the Curie-Weiss behavior for samples with large x. The paramagnetic moments from the Curie-Weiss fit of susceptibility data for heavily V-doped samples increase with x, indicating the formation of local moments with V doping. A rough estimation yields a result of $2\mu_B$ brought by one additional V ion, similar as our previous results on V-doped $BaFe_2As_2$ [12].

In order to further clarify the evolution of AFM order in $Ba(Fe_{0.92-x}Co_{0.08}V_x)_2As_2$, we performed elastic neutron scattering experiments on our samples using the Xingzhi and Kunpeng cold neutron triple-axis spectrometers. Figure 3(a) presents the **Q** scans for the AFM peak $Q = (103)$ at $T = 5$ K
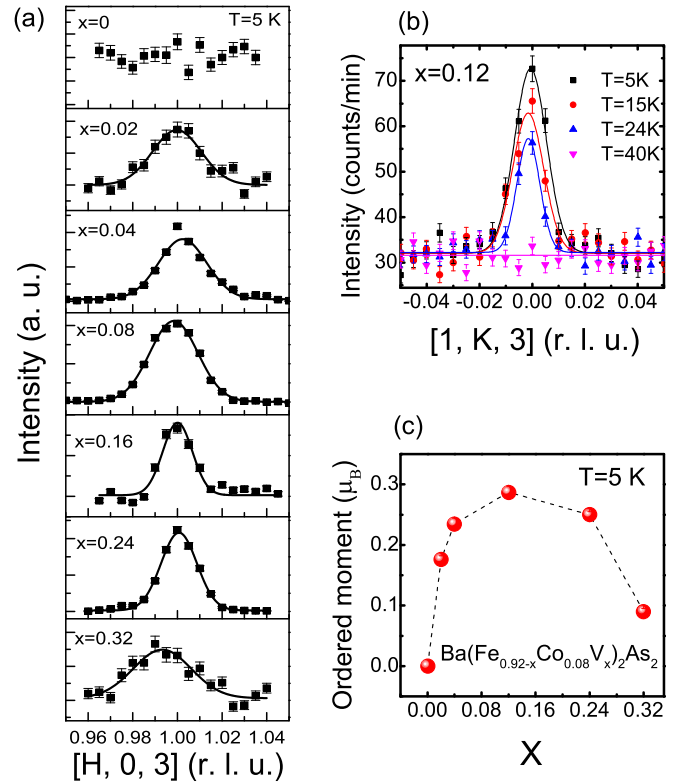
for $x = 0$, $x = 0.02$, $x = 0.04$, $x = 0.08$, $x = 0.16$, $x = 0.24$, and $x = 0.32$ along the **H** direction. All the raw data of **Q** scans are subtracted by the background above T_N. The $x = 0$ sample [namely, $Ba(Fe_{0.92}Co_{0.08})_2As_2$] has no detectable magnetic order. The following temperature-dependent measurements on $x = 0$ confirm the absence of magnetic order while the orthorhombic structural transition still exists at around $T_S = 33$ K [Figs. 4(a) and 4(b)]. The phase diagram of $Ba(Fe, Co)_2As_2$ has been extensively studied in earlier publications [5,18]. Through a detailed comparison, our $Ba(Fe_{0.92}Co_{0.08})_2As_2$ sample with a nominal Co doping of 0.08 should approximately correspond to the sample with an actual Co doping of 0.062 in the reference paper [5,18]. The properties such as T_C, magnetization, resistivity, and the behaviors of neutron data are all consistent. For the sample at this Co-doping level, it just crosses the region of the incommensurate short-range AFM phase and enters an orthorhombic paramagnetic phase below $T_S = 33$ K, as in the phase diagram drawn by Pratt *et al.* [5].

For samples with $x \geqslant 0.02$, the existence of magnetic peaks at $Q_{AFM} = (103)$ is evident. The (101) magnetic peaks were also collected for all the samples and their integrated intensities are approximately 45% of that for (103) magnetic peaks. This intensity ratio is consistent with the calculations from a C-type AFM order in $BaFe_2As_2$. For samples shown in Fig. 3(c), we also measured at least four nuclear peaks, and combined with the two magnetic peaks, the magnetic ordered moment can be determined through the refinements
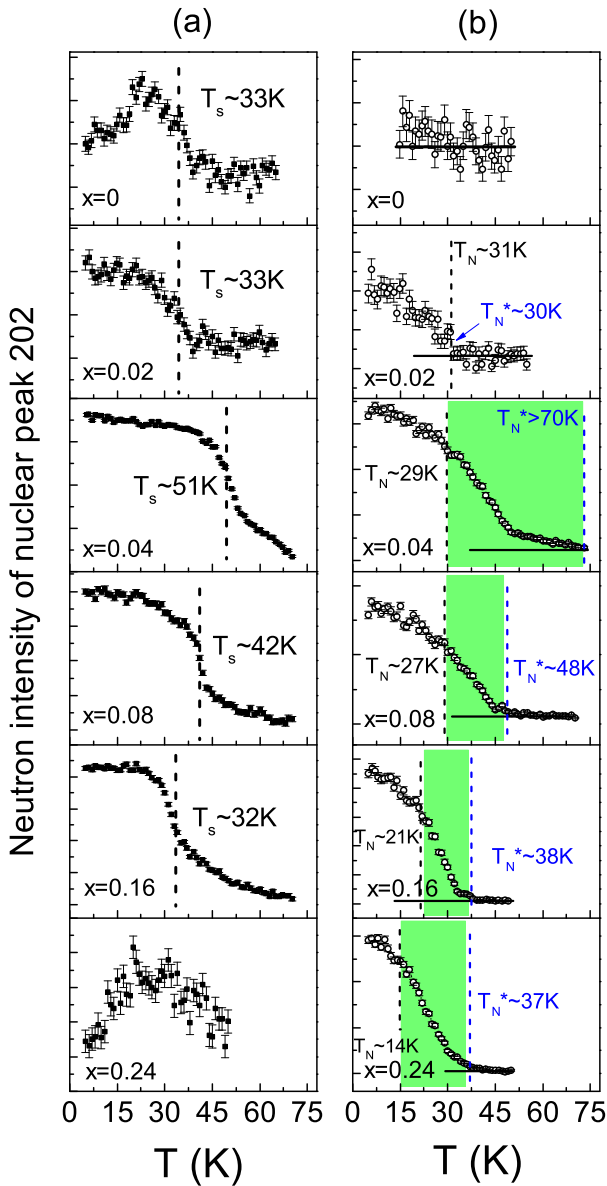
FIG. 4. Order parameters of structural and magnetic transitions in Ba(Fe$_{0.92-x}$Co$_{0.08}$V$_x$)$_2$As$_2$: (a) The temperature dependence of the neutron intensity at $Q = (202)$. (b) The temperature dependence of the neutron intensity at $Q_{\mathrm{AFM}} = (103)$. T_N^* is defined as the onset temperature of (103) peaks and T_N marks the temperature determined from the susceptibility data. The green area marks the difference between T_N and T_N^*.

FIG. 5. T-x phase diagram of Ba(Fe$_{0.92-x}$Co$_{0.08}$V$_x$)$_2$As$_2$ single crystals.

using FULLPROF software. As shown in Fig. 3(c), the ordered magnetic moments of Ba(Fe$_{0.92-x}$Co$_{0.08}$V$_x$)$_2$As$_2$ exhibit a strong domelike doping-dependent behavior with a maximum value of 0.29 μ_B; a similar evolution of moments was also reported recently in Cr-doped BaFe$_{1.9-x}$Ni$_{0.1}$Cr$_x$As$_2$ [11].

To determine the spin-spin correlation length ξ, we fit all the (103) magnetic peaks by the Gaussian function as shown by the solid lines in Fig. 3(a). The values of ξ_{ab} for V-doped samples from $x = 0.02$ to $x = 0.24$ are larger than 300 Å. For some samples, such as $x = 0.04$ and $x = 0.16$, the **L** scans for the (103) magnetic peak were also performed and fitted by the Gaussian function (data not shown here), which give a similar

result of $\xi_c > 300$ Å. The large values of ξ provide evidence for a long-range magnetic order that has been restored for the V-doped samples. In addition, the temperature dependences of a transverse **K** scan of the (103) magnetic peak for the $x = 0.12$ sample were also measured [shown in Fig. 3(b)]. Through the Gaussian fit of these peaks, the magnetic peak is confirmed to be commensurate for all measured temperatures.

In order to further investigate the AFM and structural transitions, the temperature-dependent intensities of the nuclear Bragg peak (202) and magnetic Bragg peak (103) are studied for Ba(Fe$_{0.92-x}$Co$_{0.08}$V$_x$)$_2$As$_2$, respectively (Fig. 4). For the tetragonal to orthorhombic structural transition, the neutron extinction effect from the peak splitting results in a significant change for the peak intensity of (202) around the transition temperature. However, for $x \geqslant 0.24$, the huge structural factor and strong intensity of the Bragg peaks make it difficult to figure out the structural transition because of the extinction effect [11]. The structural transition temperatures T_S are roughly determined from the maximum slope of the change of (202) intensity as shown in Fig. 4(a). The temperature evolutions of the magnetic order parameters are illustrated in Fig. 4(b). For $x = 0$, the magnetic order is indistinguishable. For $x \geqslant 0.04$, we notice that the magnetic order for most components can survive at much higher temperatures than the T_N determined from susceptibility and resistivity measurements, especially for $x = 0.04$, which exhibits a long magnetic intensity tail extending to $T > 73$ K. In Fig. 4(b), we define T_N^* as the onset temperature of the magnetic order from our neutron diffraction results and the black dashed lines mark the T_N which are determined from the susceptibility data in Fig. 2. Although for $x = 0.02$ there is almost no difference between T_N^* and T_N, the deviations of T_N^* and T_N are quite obvious for $x \geqslant 0.04$. Finally, in Fig. 5, the x-T phase diagram of Ba(Fe$_{0.92-x}$Co$_{0.08}$V$_x$)$_2$As$_2$ is based on the experimental results above.

IV. DISCUSSIONS AND CONCLUSIONS

The above experimental results confirm that the long-range C-type magnetic order as in the parent compound BaFe$_2$As$_2$ could be recovered through doping V into

$Ba(Fe_{0.92-x}Co_{0.08}V_x)_2As_2$. The ordered moments of the recovered AFM phases display a domelike evolution versus x with a maximum at around $x = 0.12$ [Fig. 3(c)]. In our previous work [12], V is shown to act as an effective hole dopant. So a straightforward explanation about the recovery of magnetic order could be based on the Fermi-surface nesting picture. Namely, the introduction of holes into the electron-doped FeAs-122 system compensates the charges by lowering the chemical potential and reshapes the Fermi surface. The better condition of Fermi-surface nesting stabilizes the magnetic ordering, and further hole doping breaks the charge balance and finally diminishes the magnetic order. Similar recoveries of the magnetic phase have been observed in Cr-doped $BaFe_{1.9-x}Ni_{0.1}As_2$ [11] and K-doped $BaFe_{2-x}Co_xAs_2$ [19], which seems to be a universal phenomenon in FeAs-122 systems. Although the Fermi-surface nesting picture of the magnetism and superconductivity in many iron pnictide and iron chalcogenide materials has been challenged, it provides a good explanation for our experimental observations.

It would be interesting to discuss some related cases in other unconventional magnetic superconducting systems. First, the magnetic order tuned by charge doping may not apply on other superconducting iron pnictides. For example, a comprehensive study on V-doped $LiFe_{1-x}V_xAs$ reveals that although the Hall coefficient of LiFeAs switches from negative to positive with V doping and angle-resolved photoemission spectroscopy (ARPES) measurements indicate a good Fermi-surface nesting between pockets carrying different orbital characters for some doping level, no magnetic order is observed in $LiFe_{1-x}V_xAs$ [15]. Second, for well-studied cuprate superconductors, the reports on doping-induced magnetic order are very rare. We find only one similar case which reported the reappearance of antiferromagnetic ordering though Zn and Ni doping on superconducting $La_{2-x}Sr_xCuO_4$ [20]. Later neutron scattering measurements confirm the recovered AFM order is La_2CuO_4 type [21]. Interestingly, an x-ray-absorption investigation on Ni-doped $La_{2-x}Sr_xCuO_4$ claims that the Ni atom can function as a hole absorber, thus tuning the charge carriers to opposite directions [22]. These findings may serve as alternative connections between Fe-based superconductors and cuprates. Although the nature of magnetism in Fe-based superconductors remains elusive, the above observations and discussions of charge tunable magnetic orders should provide insights on the final physical picture.

On the other hand, as shown in Fig. 5, the AFM ordering temperatures T_N determined from susceptibility and resistivity data are consistent (some differences of less than 5 K for $x = 0.01$ and $x = 0.02$ might be due to the fitting errors). They are around 14–30 K for all samples and exhibit a weak doping-dependent behavior. However, neutron scattering experiments reveal that the magnetic peak (103) has notable intensities at temperatures much higher than T_N for most samples. Especially for $x = 0.04$, the intensity of the magnetic peak exists even above 70 K, which is significantly larger than 29.4 K determined from the susceptibility data. The T_N obtained in $M(T)$ and $R(T)$ curves approximately corresponds to the turning point of temperature-dependent neutron intensities of (103). A similar phenomenon has been previously reported by Inosov *et al.* [23] in $Ba(Fe_{0.88}Mn_{0.12})_2As_2$, which is attributed

to the existence of a Griffiths-type AFM region of multiple coexisting phases such as AFM cluster-glass states in between T_N and T_N^* [24]. Normally these states would not generate sharp transition features in the susceptibility and resistivity curves. But they can make notable slow dynamic contributions to the magnetic peak intensities which could be detected by neutron scattering measurements. Later, Gastiasoro *et al.* [25] used a realistic five-band model with standard on-site Coulomb repulsion to study the magnetic order nucleated by magnetic impurities in iron pnictides. They found that the magnetic tails of C-type AFM modulations close to the cores of magnetic impurities may overlap with neighboring impurities and induce C-type AFM order even above T_N in a clean iron pnictide system. This provides a microscopic explanation about the enhancement of C-type AFM ordering temperature in magnetic-impurity-doped iron pnictides. Similarly, impurity-induced glassy clusters have been observed in Fe(Te,Se) systems [26–28]. So, based on the analysis above, our data strongly suggest the existence of the AFM Griffiths regime of multiple coexisting phases between T_N and T_N^* in the phase diagram of $Ba(Fe_{0.92-x}Co_{0.08}V_x)_2As_2$ as shown in Fig. 5. Besides the similar T_N deviation between the susceptibility and neutron data as reported in $Ba(Fe_{0.88}Mn_{0.12})_2As_2$ [24], more evidence is stated below. Gastiasoro *et al.*'s [25] calculations predict that the enhancement of C-type AFM order is strongly doping dependent, namely, it occurs and reaches a maximum above a certain doping concentration, and then weakens but always exists at higher doping [as shown in Fig. 1(e) of Ref. [25]]. According to the phase diagram in Fig. 5, the doping evolution of the enhanced C-type AFM ordering temperature T_N^* agrees very well with the above theoretical prediction. Namely, for $Ba(Fe_{0.92-x}Co_{0.08}V_x)_2As_2$, the enhancement of T_N^* starts at $x = 0.03$ and suddenly reaches a maximum at $x = 0.04$, and then weakens but always exists from $x = 0.08$ to $x = 0.24$. This consistency validates the physical picture provided by Gastiasoro *et al.* in explaining the phase diagram of $Ba(Fe_{0.92-x}Co_{0.08}V_x)_2As_2$, which reflects a cooperative behavior of the magnetic impurities and the conduction electrons mediating the Ruderman-Kittel-Kasuya-Yosida (RKKY) interactions between them. Our observations seem to be experimental evidence for the theoretical predictions made by Gastiasoro *et al.* [25] about the doping-dependent behavior of magnetic-impurity-enhanced AFM order. Most of the experimental reports about Griffiths-like phases are concerned with ferromagnetic materials [23], while the observations of such phases in antiferromagnets are very rare. So $Ba(Fe_{0.92-x}Co_{0.08}V_x)_2As_2$ could serve as another system for further research on exotic magnetic interactions. On the other hand, the search for possible nematic or orbital fluctuations in this system could be stimulated in the future, which may provide more explanations and insights on the above exotic phenomena.

In summary, the phase diagram of $Ba(Fe_{0.92-x}Co_{0.08}V_x)_2As_2$ has been investigated using x-ray, transport, magnetic susceptibility, and neutron scattering measurements. The vanadium magnetic impurity could quickly suppress the superconductivity of $Ba(Fe_{0.92}Co_{0.08})_2As_2$ and restore a long-range C-type AFM order. The evolution of AFM ordered moments exhibits a domelike behavior with V doping, indicating a Fermi-surface nesting picture of

ACKNOWLEDGMENTS

magnetism in FeAs-122 systems. On the other hand, the evolution of doping-dependent AFM ordering temperatures reveals the possible existence of AFM Griffiths-type phases in Ba(Fe$_{0.92-x}$Co$_{0.08}$V$_x$)$_2$As$_2$, which also provides as experimental evidence for the previous theoretical prediction based on the RKKY interactions. The above results demonstrate the rich physics when vanadium magnetic impurities are introduced into iron pnictide superconductors, which may shed light on understanding the Fe-based superconducting mechanism.

[1] P. Dai, Rev. Mod. Phys. **87**, 855 (2015).

[2] W. Bao, Chin. Phys. B **22**, 087405 (2013).

[3] M. Rotter, M. Tegel, and D. Johrendt, Phys. Rev. Lett. **101**, 107006 (2008).

[4] Q. Huang, Y. Qiu, W. Bao, M. A. Green, J. W. Lynn, Y. C. Gasparovic, T. Wu, G. Wu, and X. H. Chen, Phys. Rev. Lett. **101**, 257003 (2008).

[5] D. K. Pratt, M. G. Kim, A. Kreyssig, Y. B. Lee, G. S. Tucker, A. Thaler, W. Tian, J. L. Zarestky, S. L. Bud'ko, P. C. Canfield *et al.*, Phys. Rev. Lett. **106**, 257001 (2011).

[6] X. Lu, H. Gretarsson, R. Zhang, X. Liu, H. Luo, W. Tian, M. Laver, Z. Yamani, Y.-J. Kim, A. H. Nevidomskyy *et al.*, Phys. Rev. Lett. **110**, 257001 (2013).

[7] F. Waßer, A. Schneidewind, Y. Sidis, S. Wurmehl, S. Aswartham, B. Büchner, and M. Braden, Phys. Rev. B **91**, 060505(R) (2015).

[8] J. M. Allred, K. M. Taddei, D. E. Bugaris, M. J. Krogstad, S. H. Lapidus, D. Y. Chung, H. Claus, M. G. Kanatzidis, D. E. Brown, J. Kang *et al.*, Nat. Phys. **12**, 493 (2016).

[9] K. Marty, A. D. Christianson, C. H. Wang, M. Matsuda, H. Cao, L. H. VanBebber, J. L. Zarestky, D. J. Singh, A. S. Sefat, and M. D. Lumsden, Phys. Rev. B **83**, 060509(R) (2011).

[10] G. S. Tucker, D. K. Pratt, M. G. Kim, S. Ran, A. Thaler, G. E. Granroth, K. Marty, W. Tian, J. L. Zarestky, M. D. Lumsden *et al.*, Phys. Rev. B **86**, 020503(R) (2012).

[11] D. Gong, T. Xie, R. Zhang, J. Birk, C. Niedermayer, F. Han, S. H. Lapidus, P. Dai, S. Li, and H. Luo, Phys. Rev. B **98**, 014512 (2018).

[12] X.-G. Li, J.-M. Sheng, C.-K. Tian, Y.-Y. Wang, T.-L. Xia, L. Wang, F. Ye, W. Tian, J.-C. Wang, J.-J. Liu *et al.*, Europhys. Lett. **122**, 67006 (2018).

[13] A. S. Sefat, G. D. Nguyen, D. S. Parker, M. M. Fu, Q. Zou, A.-P. Li, H. B. Cao, L. D. Sanjeewa, L. Li, and Z. Gai, Phys. Rev. B **100**, 104525 (2019).

[14] P. Cheng, H. Zhang, W. Bao, A. Schneidewind, P. Link, A. Grünwald, R. Georgii, L. J. Hao, and Y. T. Liu, Nucl. Instrum. Methods A **821**, 17 (2016).

[15] L. Y. Xing, X. Shi, P. Richard, X. C. Wang, Q. Q. Liu, B. Q. Lv, J.-Z. Ma, B. B. Fu, L.-Y. Kong, H. Miao *et al.*, Phys. Rev. B **94**, 094524 (2016).

[16] R. Zhang, D. Gong, X. Lu, S. Li, P. Dai, and H. Luo, Supercond. Sci. Technol. **27**, 115003 (2014).

[17] P. Cheng, B. Shen, J. Hu, and H.-H. Wen, Phys. Rev. B **81**, 174529 (2010).

[18] N. Ni, M. E. Tillman, J.-Q. Yan, A. Kracher, S. T. Hannahs, S. L. Bud'ko, and P. C. Canfield, Phys. Rev. B **78**, 214515 (2008).

[19] V. Zinth, T. Dellmann, H. Klauss, and D. Johrendt, Angew. Chem. Int. Ed. **50**, 7919 (2011).

[20] T. Machi, I. Kato, R. Hareyama, N. Watanabe, Y. Itoh, N. Koshizuka, S. Arai, and M. Murakami, Physica C: Superconductivity **388-389**, 233 (2003).

[21] H. Hiraka, T. Machi, N. Watanabe, Y. Itoh, M. Matsuda, and K. Yamada, J. Phys. Soc. Jpn. **74**, 2197 (2005).

[22] H. Hiraka, D. Matsumura, Y. Nishihata, J. Mizuki, and K. Yamada, Phys. Rev. Lett. **102**, 037002 (2009).

[23] R. B. Griffiths, Phys. Rev. Lett. **23**, 17 (1969).

[24] D. S. Inosov, G. Friemel, J. T. Park, A. C. Walters, Y. Texier, Y. Laplace, J. Bobroff, V. Hinkov, D. L. Sun, Y. Liu *et al.*, Phys. Rev. B **87**, 224425 (2013).

[25] M. N. Gastiasoro and B. M. Andersen, Phys. Rev. Lett. **113**, 067002 (2014).

[26] W. Bao, Y. Qiu, Q. Huang, M. A. Green, P. Zajdel, M. R. Fitzsimmons, M. Zhernenkov, S. Chang, M. Fang, B. Qian *et al.*, Phys. Rev. Lett. **102**, 247001 (2009).

[27] T. J. Liu, J. Hu, B. Qian, D. Fobes, Z. Q. Mao, W. Bao, M. Reehuis, S. A. J. Kimber, K. Prokes, S. Matas *et al.*, Nat. Mater. **9**, 718 (2010).

[28] V. Thampy, J. Kang, J. A. Rodriguez-Rivera, W. Bao, A. T. Savici, J. Hu, T. J. Liu, B. Qian, D. Fobes, Z. Q. Mao *et al.*, Phys. Rev. Lett. **108**, 107002 (2012).